Geodetic contributions to the Alaska Hazard Maps: Collaborative Research between the University of Alaska Fairbanks and Purdue University

G15AP00051 to University of Alaska Fairbanks
G15AP00056 to Purdue University
Period Covered: April 1, 2015 to December 31, 2016 (including no-cost extension)

Julie Elliott, Department of Earth and Planetary Sciences, Purdue University, 550 Stadium Mall Drive, West Lafayette, IN 47907

Jeff Freymueller, Geophysical Institute, University of Alaska Fairbanks, 2156 Koyukuk Drive, Fairbanks, AK 99709

Abstract

We have developed the first complete elastic block model to describe the tectonic motions of Alaska and adjacent areas of the Canadian Cordillera. The model includes 24 blocks in addition to the Pacific and North American plates, with block-bounding faults chosen based on available information for active faults and seismicity, as well as strain concentrations observed in the GPS velocity field. The model was constrained mainly by GPS velocities estimated from ~25 years of data, with uncertainties incorporating a colored noise model and models for non-tectonic motions removed. Overall, the model fits the data with a reduced chi-square of 4.2, indicating an average residual of about twice the data uncertainty. The observed motions are well described by the motion of rigid blocks for the areas far from the main Pacific/Yakutat/North America plate boundary, but misfit is larger in the areas of more intense tectonic deformation. This might result from inadequate correction models for non-tectonic deformation or transient events, or deformation that is more distributed than block-like.

Introduction

We proposed to contribute to the Alaska Hazard Maps update by developing an updated, unified GPS-derived tectonic model for Alaska. As part of this process, we proposed to develop one or more block models to explain the deformation across all of Alaska, building on the efforts we have already made in several specific sub-regions. The block models are constrained by an updated Alaska-wide GPS velocity field, corrected for non-tectonic components including a Glacial Isostatic Adjustment correction model and a 1964 postseismic model. For some data, we also needed to include a correction model for postseismic deformation following the 2002 Denali fault earthquake. We had originally proposed to develop improved correction models, but this proved more challenging than anticipated. The best available models were used and are summarized in this report.

After developing the velocity field, we carried out a series of experiments in modeling different regions of Alaska using regional or simplified block models. These were ultimately integrated into a single Alaska-wide block model. This model is a good representation of tectonic motions across all of Alaska, although a few specific areas remain challenging to model, because of the number and complexity of transient events, earthquakes, or other time-dependent effects, or because of features in the data that remain difficult to explain. Deformation in the transition from the collision process in the St. Elias through Prince William Sound and Cook Inlet is complex and we think that model improvements are definitely possible there. The postseismic deformation from the 2002 Denali fault earthquake remains a problem for our modeling as well, and when a good postseismic model is finally complete we expect it will require adjustments to the block model in the southcentral Alaska region, and perhaps north across the Denali fault.

Work on the model was delayed for a number of reasons, mainly associated with unanticipated delays involving graduate students. As a result, the work went into a no-cost extension and model integration and improvement has been an ongoing process. Thus this report is somewhat late, but does incorporate many new developments and improvements made over the last year.

Dealing with the substantial number of slow slip events, earthquakes, and postseismic transients remains for future work. Some existing GPS data in key areas cannot be used or can only be used in part because models for these time-dependent phenomena are not yet good enough to make full use of all observations. The current block model was developed using software developed by Julie Elliott (originally during her graduate work, with continued development afterward). Portions of the model have been transferred to the open source *Blocks* code, developed by Brendan Meade and Jack Loveless (Meade and Loveless, 2009). *Blocks* is a powerful code, but there are some challenges in translating fault models into the formats it demands. Eventually the entire model will be converted for use with *Blocks*.

GPS Velocity field

We based our GPS velocity field on the complete set of solutions analyzed by UAF, up to fall 2016. These solutions include data for all sites in and around Alaska that we have been able to find, both continuous and episodic (campaign) sites. The entire solution series, which extends back to the beginning of 1992, has been analyzed using the same models and approach, using the GIPSY/OASIS software. Daily solutions were aligned with the ITRF2008 reference frame, and then velocities were fit to each individual stations' time series, accounting for seasonal variations, offsets and so on.

Daily solutions and Reference Frame Alignment

We analyzed all data using the GIPSY/OASIS goa-5.0 software used in point positioning mode. We used the standard solution strategy described in Fu and

Freymueller (2011). Each day of data from each station was processed independently, and all stations for a given day were merged together into a combined solution, which was then aligned with the ITRF2008 frame.

Individual daily solutions used both phase and pseudorange data. We used data decimated to a 5 minute interval (6 minutes before 1996), and removed a standard set of time dependent sub-daily models for earth tides and ocean tidal loading. The ocean tidal loading model was computed from the TPXO.7 global tidal model using the SPOTL software (Agnew, 1997), computed in the center of mass of Earth System frame (CM). See Fu et al. (2011) and Fu and Freymueller (2012) for details.

We fixed the satellite orbit and clock parameters to those provided by JPL, using their "non-fiducial" solution (based on a free network solution with only loose constraints on all station positions). For data after 2009, we used the JPL daily contributions to the International GNSS Service (IGS). For earlier data, back to 1996, we used the JPL submission to the first IGS reprocessing campaign, which used the same analysis strategy and software as the post-2009 products. For data before 1996, we used a global network and estimated orbits and clock errors ourselves. For each station, we estimated the coordinates for the day along with nuisance parameters for the receiver clock bias (every epoch) and a time-dependent tropospheric delay. We estimated a time-dependent zenith tropospheric delay (varying in time assuming a random walk noise model), and two single daily tropospheric gradient parameters.

The reference frame alignment was computed daily, using a large set of ITRF2008 frame sites. We maintain a list of sites for which the ITRF2008 coordinate model remains valid, so that sites displaced by earthquakes, antenna changes or other physical offsets, or other unmodeled effects in the data do not bias the frame alignment. The ITRF2008 coordinate model was evaluated for each day of data, and then our free-network solution was aligned to the ITRF2008 coordinates using a 7-parameter Helmert transformation.

Velocity Estimation

Many sites in Alaska suffer from offsets or non-linear motions due to earthquakes, slow slip events, and postseismic transients. All sites also have a strong seasonal motion, primarily in the vertical component, due to surface loading primarily associated with snow and hydrology (Fu and Freymueller, 2012). Because the basic concept of an elastic block model is to model the steady motions of the sites, we were careful to select the data for each site that we think is representative of that steady motion, and unbiased by displacements caused by earthquakes or transient events.

We used the full set of data from each site whenever possible. For sites very close to the Denali fault, we used only the pre-earthquake data (before November 2002) because the postseismic deformation is very large compared to the steady

motion. For sites in the St. Elias region of southern Alaska and the Yukon, we applied a postseismic adjustment for the Denali earthquake as discussed in *Elliott et al.* 2013. For sites in southeast Alaska that show a postseismic signal from recent earthquakes, we truncated the data at the time of the 2012 Haida Gwaii earthquake, or in some cases the 2013 Craig earthquake. For more distal sites, we estimated an offset for the earthquake but continued to use the post-earthquake data. Campaign sites from Augustine Island use only data from before its 2006 eruption, while the PBO sites use only data after the eruption (there is no sign of any volcanic deformation in these data). This approach implicitly assumes that the non-volcanic deformation sources are stationary in time. We had to use special care for other sites in the Cook Inlet area, due to the several very large multi-year slow slip events. We rejected some data from Upper Cook Inlet because there were simply too many conflicting time-dependent events. For most sites in Cook Inlet, our velocities average over the whole time interval, which includes two large slow slip events. Thus there is some inconsistency in the velocity field here that results from the different temporal sampling of each site, although we have removed the most extreme cases.

We fit each site's 3D time series based on a simple parametric model of linear motion with time, sometimes with other terms added. We removed a model for seasonal motions derived from the GRACE mission from all sites. This model uses a non-parametric approach to estimating the seasonal motions, removing the long-term trend from the displacements predicted from the GRACE loading model, stacking the residuals by time of year and then smoothing them to derive the seasonal correction (Freymueller, 2009; Zou et al., 2014). For continuous sites we also estimated a residual seasonal correction including annual and semi-annual harmonic terms. We estimated offsets in the time series for earthquakes or other events that cause sudden displacements, such as antenna changes. We did not add parametric models for slow slip events or postseismic deformation, but rather attempted to minimize or avoid these signals through the choice of the time window for the affected sites. Unfortunately, some inconsistencies remain in the Cook Inlet region due to the multiple slow slip events.

The site velocities in ITRF2008 were then transformed into velocities relative to the North American plate. The transformation has two components, the main one being removing a single rotation that describes the motion of the North American plate in ITRF. The second component is a small translation to account for the estimated difference between the frame origin of ITRF and the center of plate rotation. This small correction, slightly less than 1 mm/yr and primarily along the Earth's spin axis, reflects a combination of error in the definition of the ITRF frame, the effects of global-scale deformation (for example, GIA) that is not accounted for in the ITRF development, plus measurement error in the estimation of the geocenter. We used an estimate based on Argus et al. (2010). With the removal of both of these effects, we have velocities relative to the North American plate.

Correction Models

Correction models were applied for the major non-tectonic components. We had originally proposed to develop new and updated models but this proved to be impractical. The 1964 postseismic deformation affects primarily the horizontal, while the Glacial Isostatic Adjustment (GIA) model affects primarily the vertical, but with horizontal displacements of ~1 mm/yr over a broad region and up to several mm/yr immediately around the main ice loads.

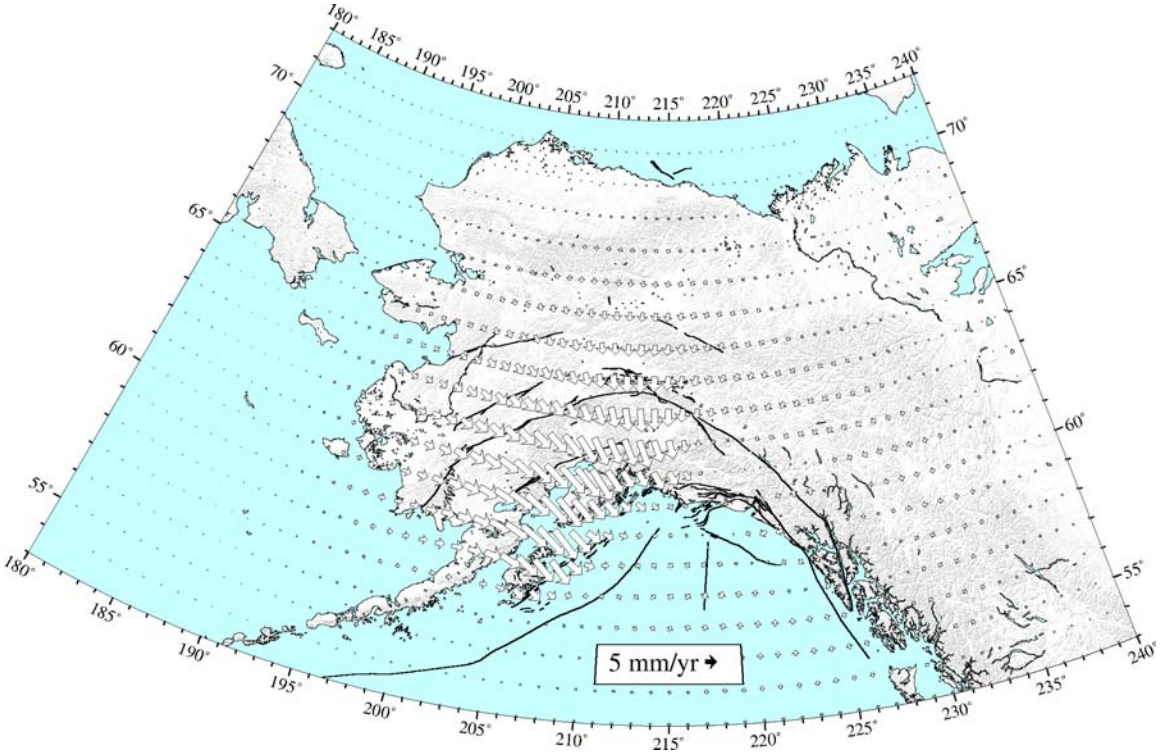

Figure 1. Non-steady state tectonic correction model for the horizontal velocities shown on a 1° by 1° grid, including both 1964 postseismic displacement and GIA. The horizontal velocities are dominated by 1964 postseismic deformation. At this grid resolution, this figure does not represent the complex pattern of corrections adjacent to the main ice loads, which can reach several mm/yr. See Elliott et al. (2010) for a closer view of that component, although the model has been updated and is not exactly the same as the one shown in that paper.

1964 Postseismic Deformation. We used the 1964 postseismic model developed by Suito and Freymueller (2009). This model was based on a 3D finite element model that includes a dipping slab, and a Newtonian asthenospheric viscosity. The model was optimized to fit GPS velocities from central Alaska, in combination with an elastic deformation model for the locked subduction zone. Suito and Freymueller (2009) estimated a best-fitting relaxation time of ~20 years (uncertainty range 15-25 years), corresponding to an asthenospheric viscosity of $\sim 10^{19}$ Pa-sec. The model was evaluated on a grid of locations and is available as a gridded correction model that can be interpolated to any desired location.

Glacial Isostatic Adjustment. GIA was modeled based on the model developed by Hu and Freymueller (in preparation), which is an evolution of the model of Larsen et al. (2005) and Elliott et al. (2010). The main component of this model is the response to the post-Little Ice Age deglaciation of Alaska. It includes smaller components from the post-Last Glacial Maximum deglaciation for Alaska and for the Laurentide ice sheet. The model was evaluated on a grid of locations and is available as a gridded correction model that can be interpolated to any desired location.

Combined Model. The combined non-tectonic correction model was computed by summing together the two models described above. A coarse-resolution version of this model is shown in Figure 1; the model is dominated by 1964 postseismic deformation in the horizontal. The main pattern in the horizontal is that a broad region of southern and western Alaska experiences a trenchward motion back toward the 1964 rupture zone. In western Alaska, this can exceed 5 mm/yr. The predicted non-tectonic motions decline to near zero near the Arctic coast. This gridded model was interpolated to all site locations to provide a velocity correction.

The impact of the correction model for 1964 postseismic deformation is substantial, especially in western Alaska where it is comparable to or larger than the observed velocities. As a result, the application of the correction model completely changes the pattern of velocities, and reveals a coherent underlying tectonic pattern (Figure 2). The corrected velocity field was used in all subsequent modeling.

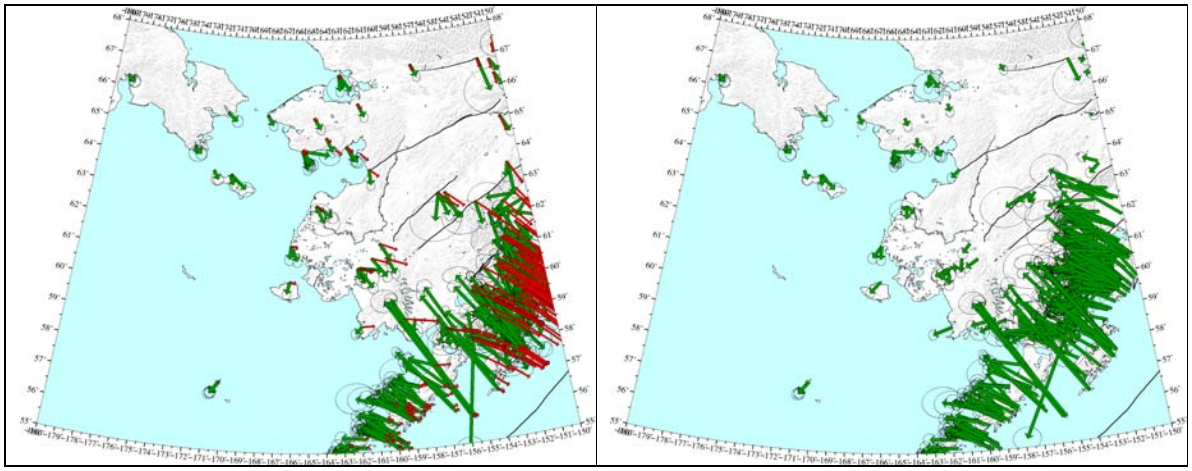

Figure 2. Velocities for western Alaska and 1964 postseismic correction. (left) Uncorrected velocities in green with 1964 postseismic model in red. (right) Corrected velocities. The block-like motion of western Alaska is revealed when the postseismic deformation is removed.

2002 Denali fault earthquake. For sites near this event, mainly those in the St. Elias range and the Yukon, we applied a correction for the postseismic deformation due to the 2002 Denali fault earthquake. We used the empirical correction model

developed by Elliott et al. (2013) because a satisfactory forward model for the postseismic transient does not yet exist.

Results

We estimated velocities for a total of 1139 sites in and around Alaska. (many of these sites are outside of the core model region, but the complete velocity field is given in the appendix for completeness). All models were developed using the velocities relative to the North American plate as described above, with the non-tectonic models removed. The velocity field used for modeling was much smaller, excluding sites outside the main region of interest and also some sites in areas like the Alaska Peninsula where a graduate student was completing their thesis work (Li and Freymueller, in press).

Initial Model Exploration

Initially, we carried out a series of experiments in modeling different regions of Alaska using regional or simplified block models. These were ultimately integrated into a single Alaska-wide block model. These test models were divided regionally between the PIs, with Freymueller being responsible for northern and western Alaska, including the Alaska Peninsula and the Aleutians. Elliott was responsible for integrating models in southeastern and eastern Alaska, and then integrating these with the model Freymueller had previously developed for Prince William Sound and the Cook Inlet area. After these initial tests, Elliott was responsible for integrating all of these parts and pieces into the final model. This final step proved to be fairly simple for some parts of Alaska, but extremely complex for other regions (mainly southcentral Alaska, including the western St. Elias, Prince William Sound, Cook Inlet, and Kodiak Island).

Northern and Western Alaska

The velocity field for northern and western Alaska (Figure 3) shows a clear block-like pattern. Velocities of sites on the North Slope of Alaska are quite small relative to North America, but on average are non-zero (and directed to the SE). On the Seward Peninsula, velocities are directed to the SSE, and sites in the Russian Far East show a coherent block-like rotation pattern that matches with the Seward Peninsula sites. The pattern of velocities changes abruptly south of the Kaltag fault, with all sites south of the Kaltag fault moving to the SW rather than the SSE. There is a remarkable ~90° rotation of the velocity field over a distance of ~100 km between the Seward Peninsula and the region south of the Kaltag fault. Unalakleet, despite being located very close to the Kaltag fault, seems to move about the same as sites well to the south of the fault.

We used evidence for Quaternary fault activity, evidence for active seismicity, and changes in the observed velocities to define an initial block model for this region. Portions of the Kaltag fault show evidence for Quaternary activity, and the seismicity catalog shows a fuzzy lineation of seismicity along portions of the fault (the catalog is poor in western Alaska due to a lack of seismic stations). We took the

Kaltag fault to be a hypothetical block boundary. The Kobuk trough, which runs along the southern part of the Brooks Range, also shows some evidence for Quaternary activity. The most recent year of seismicity, which includes data from the Alaska Transportable Array, also shows seismicity along this fault. There is a clear difference between the motion of sites on the Seward Peninsula and those on the North Slope, we selected this fault as another block boundary. The Denali fault is also likely to be active across this region, and will be dealt with later in this section.

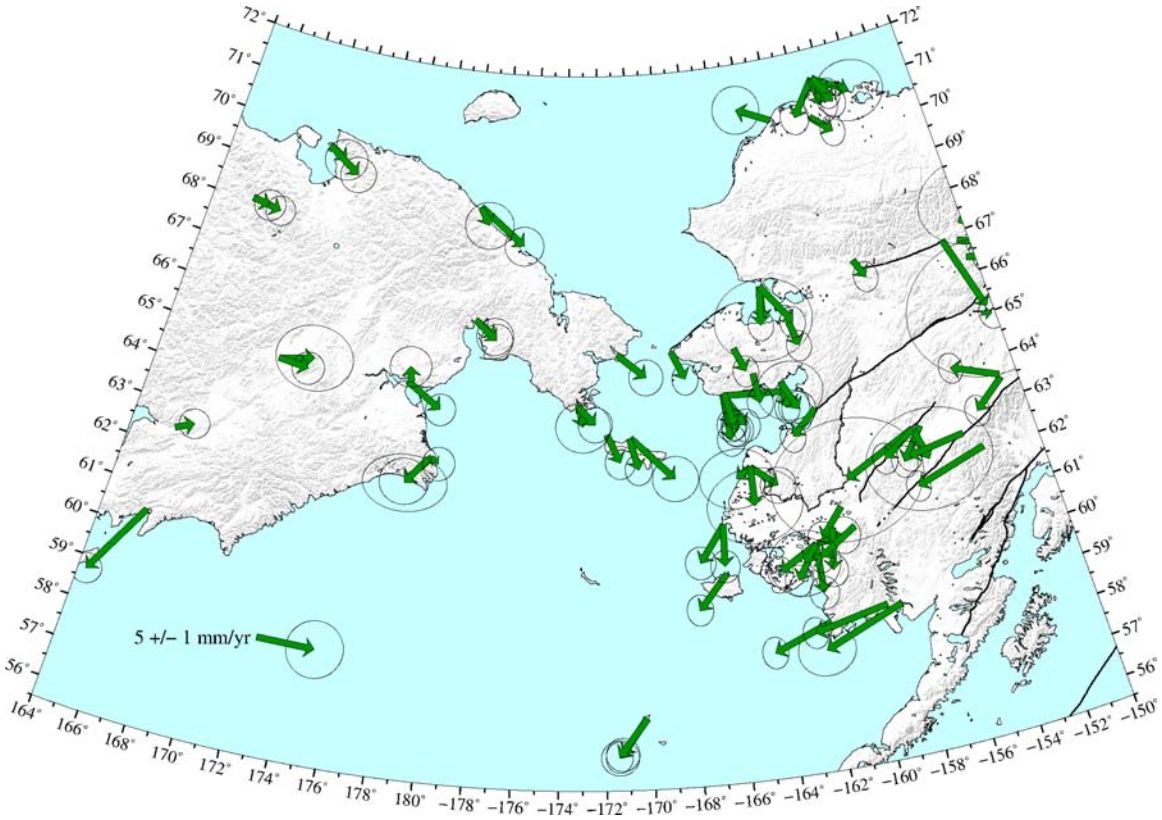

Figure 3. Corrected velocities for Northern and Western Alaska, including the Bering Sea region and the Russian Far East. Velocities for sites along the Alaska Peninsula and Kodiak Island have a large component of elastic strain from the locked subduction zone and are not shown. The southernmost sites shown here also show a clear component of subduction-related strain. Faults are taken from the Quaternary Fault and Fold database (Koehler, 2013).

We examined the velocity field more closely by selecting a set of sites that appeared to move as a rigid block and estimating and removing a rigid block rotation from the data. This allowed us to examine the spatial changes in the velocity field more closely. An example is shown in Figure 4, in which a rigid block rotation was removed based on all sites north of the Kobuk Trough and Tintina fault. Such explorations allowed us to examine motions across potential block boundaries and assess their likely importance. Note that these simple inversions ignore elastic deformation from locked faults, but in this case the impact is small because the slip rates are low and the sites are spaced far apart and generally far from the faults.

However, sites located further south definitely have a much larger elastic strain component from the subduction zone and other tectonic features in southern Alaska, and accurate block motions for that region can be estimated only from models that incorporate the elastic strain from the locked subduction zone.

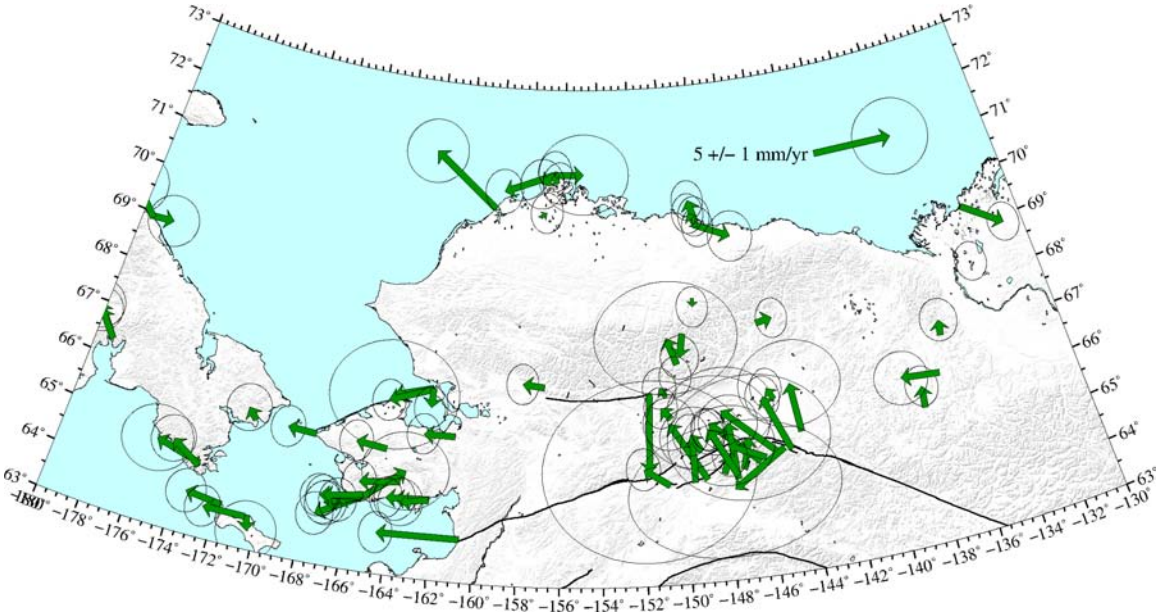

Figure 4. Velocities relative to a block defined by all sites north of the Tintina fault and Kobuk Trough. Sites on the Seward Peninsula all move westward relative to this block, suggesting strike slip motion on the Kobuk Trough perhaps with a component of extension in its western part. Sites in the SE part of the figure include an elastic strain component from the subduction zone and faults further to the south. Faults are taken from the Quaternary Fault and Fold database (Koehler, 2013).

After a variety of such experiments, we identified three main blocks to be represented in the model: Arctic, Bering Sea, and Kuskokwim. The Kobuk Trough separates the Arctic and Bering Sea blocks, while the Kaltag fault separates the Bering Sea and Kuskokwim blocks. The southern boundary of the Kuskokwim block was taken to be the Denali fault. St. Paul island in the Bering Sea was assumed to lie on the Kuskokwim block. Figure 5 shows velocities relative to the Kuskokwim block, with a further correction applied for the elastic deformation from the locked subduction zone, taken from an extension of the model of Li et al. (2016). In this frame, sites north of the Kaltag fault show coherent eastward to northeastward motion. Sites south of the Denali fault clearly move to the west or southwest. While the elastic model is clearly not perfect, given the systematic residuals of sites on the Alaska Peninsula, the elastic deformation would be directed roughly orthogonally to the motion of the sites south of the Denali fault, indicating that the motions of these sites must include a component of block motion and not just subduction strain. We then carried out further experiments using the Peninsula block motion (described in the next section), and concluded that a total of five blocks were required to explain

the motions in this region, from north to south: Arctic, Bering Sea, Kuskowkim, Naknek, and Peninsula.

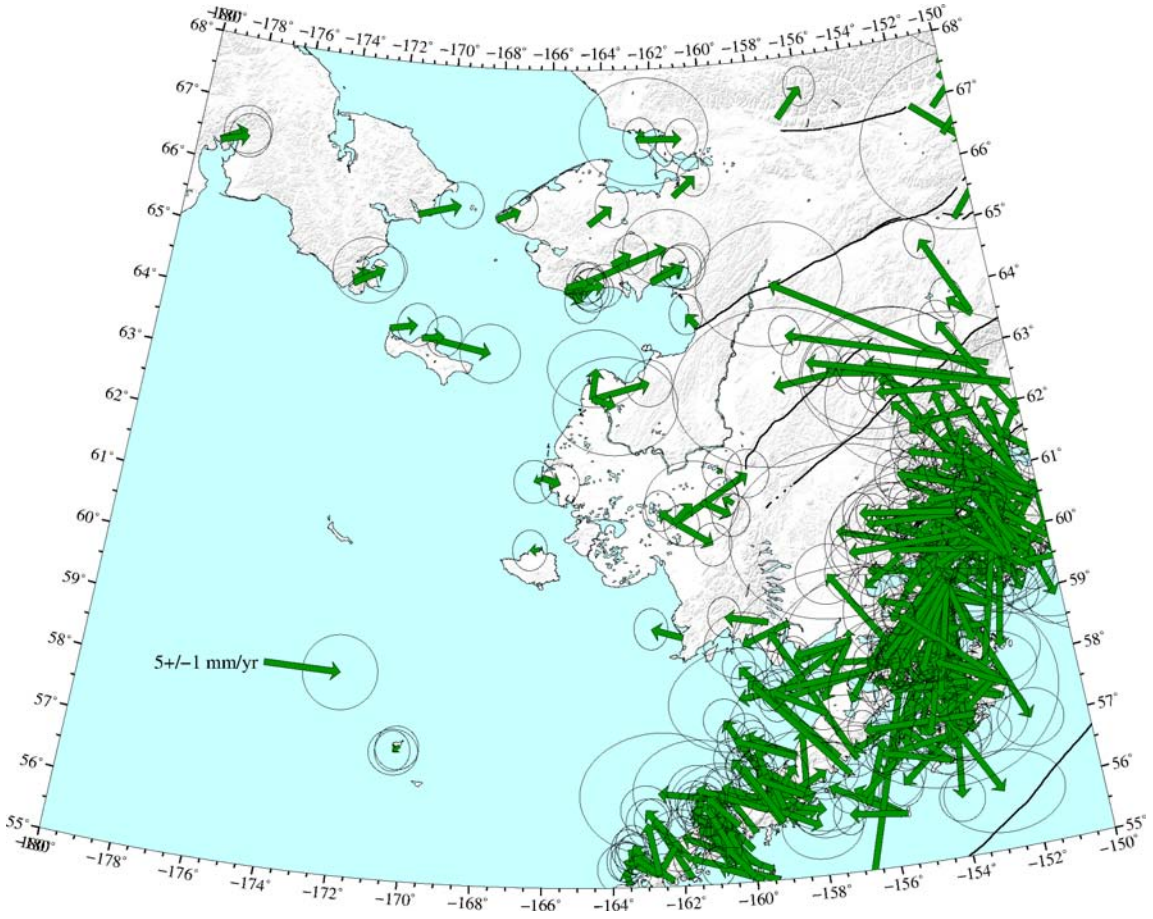

Figure 5. Velocities relative to the Kuskokwim block defined by all sites between the Tintina fault and Denali fault. An elastic model for the locked subduction zone has been removed based on Li et al. (2016). Sites on the Seward Peninsula all move westward relative to this reference, suggesting strike slip motion on the Kobuk Trough with a component of extension in its western part. Sites in the SE part of the figure include an elastic strain component from the subduction zone and faults further to the south. Faults are taken from the Quaternary Fault and Fold database (Koehler, 2013).

Alaska Peninsula and the Aleutian Arc

The Alaska Peninsula features a dramatic along-strike change in the extent of the locked part of the subduction thrust zone, and thus large along-strike changes in deformation (Fletcher et al., 2001; Fournier and Freymueller, 2007; Li and Freymueller, in press). The elastic deformation from the locked subduction zone is combined with a roughly strike-parallel transport of the Alaska Peninsula itself (Cross and Freymueller, 2008; Freymueller et al., 2008; Li and Freymueller, in press). Notably, there is a segment at the end of the Alaska Peninsula where the strain associated with the subduction zone is zero within a very small tolerance, so that velocities there are described entirely by a rigid block rotation. There is another

such area around Dutch Harbor in the eastern Aleutians and a third near Atka in the central Aleutians (Freymueller et al., 2008; Li and Freymueller, submitted).

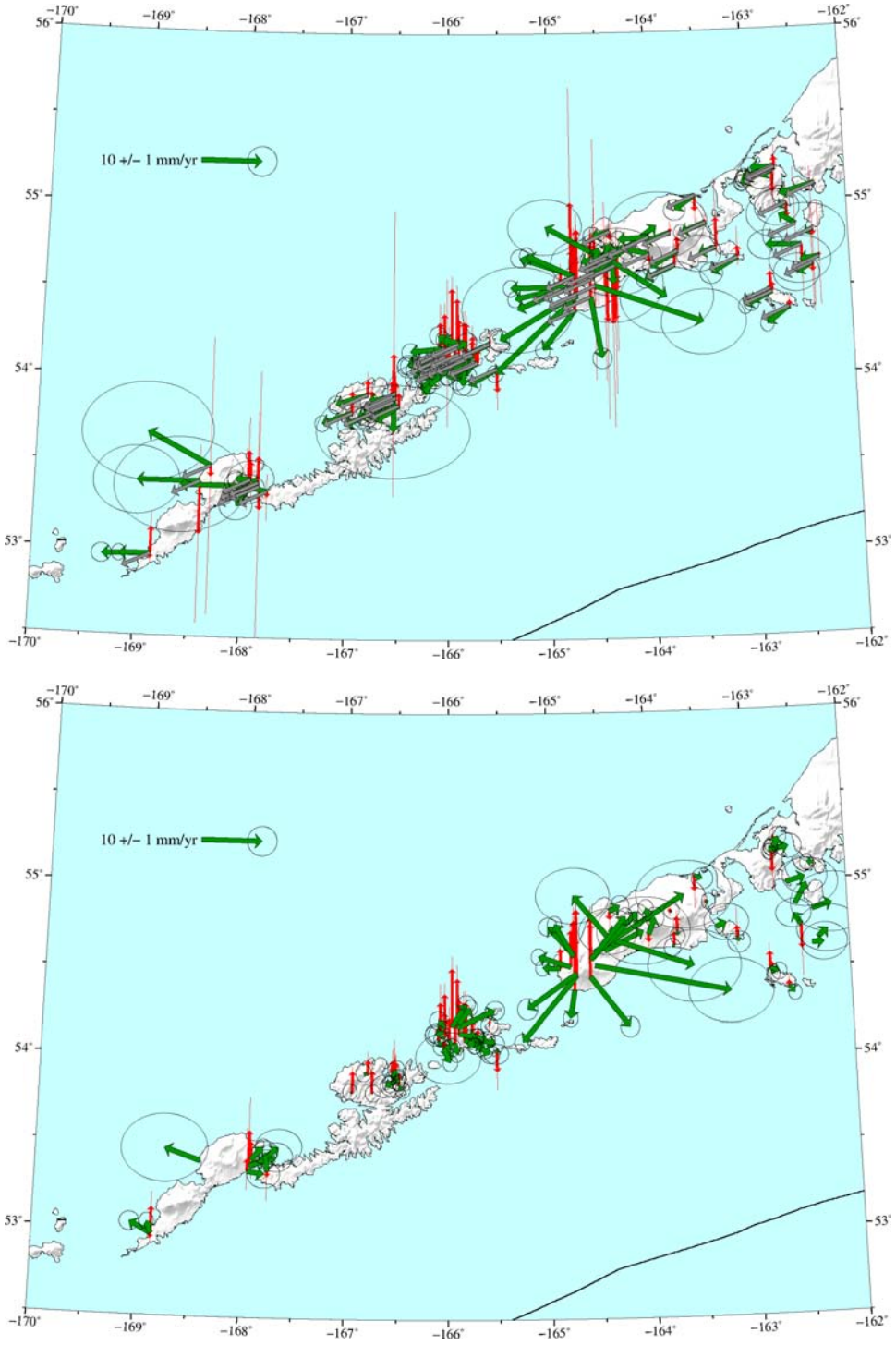

Figure 6. Velocities in the Alaska Peninsula and eastern Aleutians. (top) Velocities (green vectors) are relative to North America, and the gray vectors are the predicted Peninsula Block motions. (bottom) Residual velocities after subtracting the predicted Peninsula Block motions. Between 164°W and 167°W, all residual velocities are

essentially zero except for those located around active volcanoes. Red vectors show the vertical motions.

We tested a series of models to explain the velocities observed along the Alaska Peninsula, mainly using the TDEFNODE software. The final versions of those models are presented in Li and Freymueller (in press). We tested models in which the Alaska Peninsula and Cook Inlet were part of the same block (the Peninsula Block of Li et al., 2016), along with various other combinations of Cook Inlet, the Alaska Peninsula and the eastern and central Aleutians. We found that the best definition for the Peninsula Block included the zero strain region near Cold Bay at the end of the Alaska Peninsula, sites in the Dutch Harbor area that are not affected by the active Akutan and Okmok volcanoes, and sites near Atka in the central Aleutians. Sites in these three locations are well fit by a single rigid block rotation, which produces nearly trench-parallel block motions in the Alaska Peninsula and eastern Aleutians (Figure 6), and motion with both a trench-parallel and trenchward component in the central Aleutians. In all cases, the estimated Peninsula Block motions are very close to the estimated arc velocities derived by Cross and Freymueller (2008) from modeling the subduction strain component.

We concluded based on these experiments that nearly the entire Alaska Peninsula and the Aleutian arc east of Amchitka Pass likely move as a single rigid block that rotates southwestward relative to North America. This description applies to the land areas; as pointed out by Cross et al. (2008), it is likely that slip partitioning of oblique subduction is occurring with strike slip faults south of the Aleutian islands, at least in the central Aleutians. Our description is not inconsistent with there being an arc-parallel extensional component of deformation through this region, but suggests that such extensional deformation is overall very slow compared to the block motion. The northern boundary of the Peninsula Block is unclear, but is likely located mostly underwater where there are no GPS sites. The boundary ultimately chosen for the final model needs to be interpreted in that context.

Southeast and Eastern Alaska

The model for this region is based on the models in *Elliott et al.* (2010) and *Elliott et al.* (2013), with several important modifications. The model in the former did not have defined western boundaries and the latter did not have well-constrained eastern boundaries, so merging the two models required consideration of how best to join faults used in both. In the vicinity of Yakutat Bay and the Malaspina, where several faults presumably merge, this effort is complicated by the extremely spare data availability. Fault geometries there were chosen to be compatible with geometries to the west and southeast that were constrained by data and also to be consistent with geological and seismic data (including new data that has accumulated since the original models have been published). Several faults merge near Hubbard Glacier, which is roughly coincident with the area exhibiting the highest exhumation rates (*Enkelmann et al.*, 2015). New data added from sites the eastern Yukon (*Marechal* et al., 2015, Figure 7) and the northern Canadian

Cordillera necessitated a re-evaluation of block boundaries. In the 2010 model, of the Canadian Cordillera was part of the Northern Cordillera block. New data from the northernmost Cordillera suggest that this region is part of separate block, with a southern boundary near the southernmost extent of the Richardson Mountains. This new block is termed the Northwest Coast block (see below). Several tests were performed to see if data from a new network in the Yukon required additional block boundaries to explain. Adding additional blocks did not significantly improve the model fit to the data, so the simplest combination of blocks was chosen.

Experiments for model fit the Chugach/Interior/Prince William Sound

The model presented in *Elliott et al.* (2013) focused on the Chugach, St. Elias and western Prince William Sound regions. The northern and western boundaries were not defined and no data from these regions were included in the model. Adding in additional data to the north and west required significant changes to the existing model. Data stretching from the northwest corner of the model to the Denali fault has a clear northerly trend, suggesting a subduction related signal (Figure 8). We extended the subduction interface, which represents the interface between the Yaktuat slab and Alaska, farther north of the limits presented in *Elliott et al.* (2013). The interface provided the best fit with a high degree of coupling in the south and smaller degrees of coupling to the north. This places the subduction

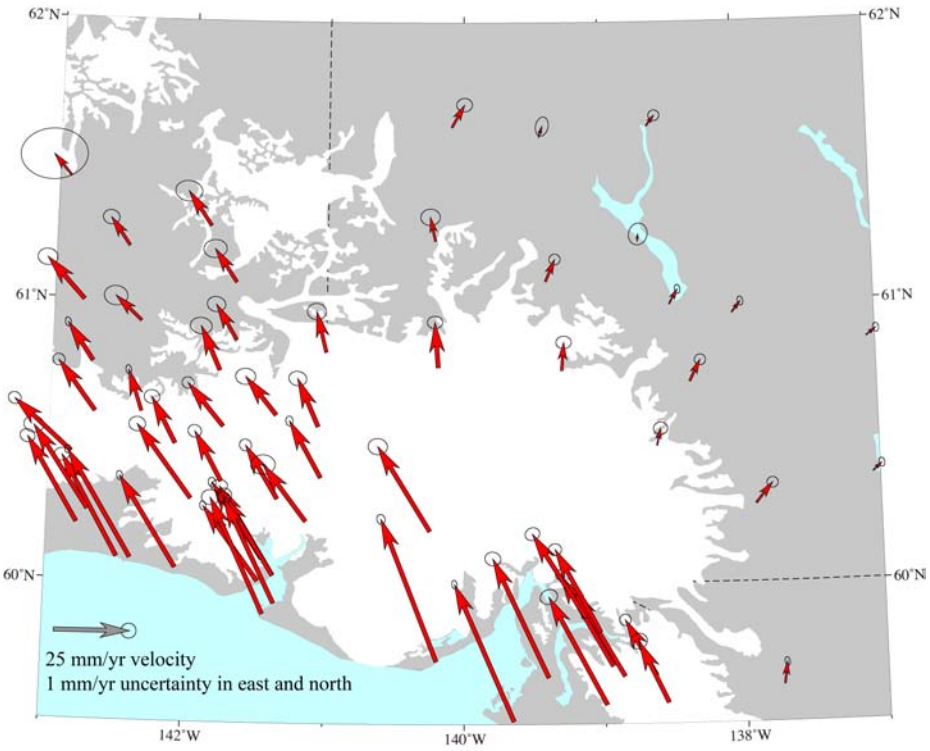

Figure 7. Velocities at sites in the Yakutat corner.

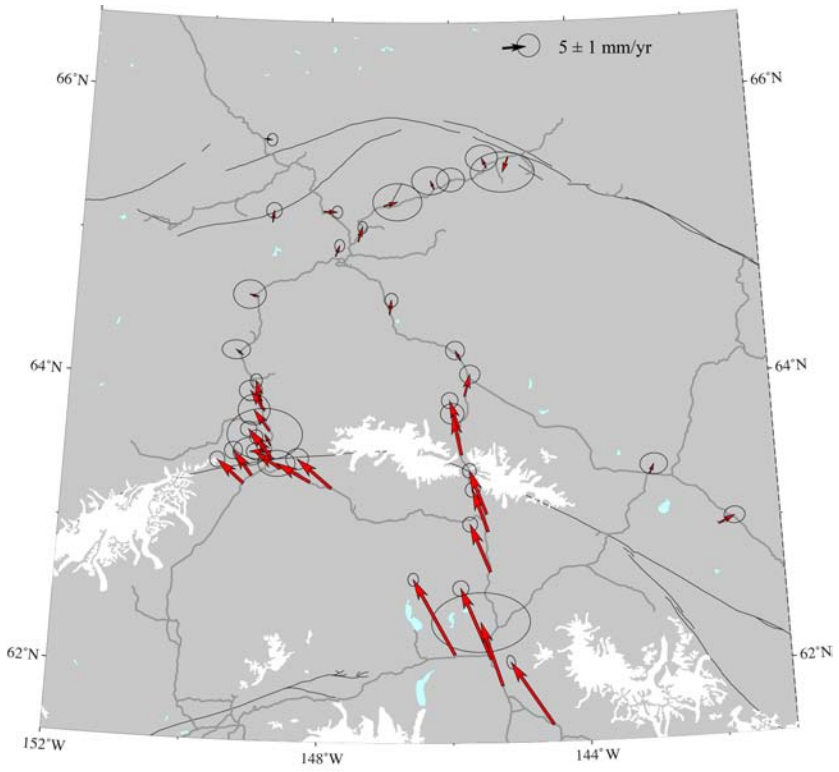

Figure 8. Velocities at sites in Interior Alaska.

interface further east and north than previous models and significantly further east than the end edge of the observed Wadati-Benioff seismicity.

As we experimented with the subduction interface, we found that the data on the upper plate south of the Denali fault could not be fit by a single block. *Elliott et al*. (2013) defined the Elias block as a counterclockwise rotating block occupying the area between the coast, the Wrangell Mountains, and an undefined point west of Prince William Sound. Previous studies (e.g. *Fletcher*, 2002) defined the whole of the region south of the Denali fault to be the counterclockwise rotating Southern Alaska block (SOAK). Predictions of block motions for the Elias block are significantly faster than those for the SOAK block of *Fletcher* (2002) and too fast for sites north of the Wrangell Mountains. Predictions for SOAK were too slow for the sites nearer the coast. To solve this problem, we divided the region by a roughly west-east trending boundary that follows the trace of the Castle Mountain fault and the western Border Ranges fault before trending more northerly to link to the junction of the Totschunda and Duke River faults. The location of the eastern part of this boundary was guided by the data, although in some regions the data was sparse. The model boundary is creeping; tests of different locking depths for the boundary concluded that any significant locking on the boundary worsened model fit to the data. At least in the east, this boundary may represent a degree of distributed deformation.

In the region between this boundary and the Denali fault, experiments were performed to test for the optimal upper plate block motion. The SOAK block of *Fletcher* (2002) fit the western half reasonable well but resulted in northward residuals in the eastern half of the region. Dividing the region into two blocks provided the best fit to the data. In the west, block motions resemble that of SOAK while in the east the motions are more northeasterly. The chosen boundary between these two blocks is somewhat arbitrary; it must be west of the eastern data profile across the Denali fault along the Richardson Highway and east of the sites along the Parks and western Denali highways. Sparseness of the data currently limits our ability to more precisely determine where the division between the blocks must be. As with the previous new boundary, this model boundary is creeping and may represent distributed deformation.

The area from Prince William Sound west has proved challenging. The slab transitions from thickened, shallowly subducting Yaktuat block to the more steeply dipping Pacific plate. The depth of the model slab planes was guided by seismicity and consistent with the slab interface in *Elliott et al.* (2013), which assumed that the top of the slab coincided with the depth to the top of Yakutat basement as estimated through offshore seismic data analysis. Several options for the change from Yakutat slab motion to Pacific slab motion were tested and evaluated in terms of fit to the GPS data. The best fit to the data was obtained when the transition occurred roughly beneath the middle of the Kenai Peninsula. This result, based solely on fit to the GPS data, agrees well with the seismically imaged transition discussed in *Kim et al.* (2014).

Upper plate motion in this area is complex. *Elliott et al.* (2016) had the Elias block extending through Prince William Sound, although sites at the western end of the model were not well fit, displaying residuals indicating that block motion with a larger western component was required. Assigning all of the region between the Bering Glacier and Kodiak Island to the Elias block resulted in a poor overall model fit to the data and in particular, westward residuals at sites between Prince William Sound and Kodiak Island. The estimated Peninsula block motion discussed above and in *Li et al*. (2016) and Li and Freymueller (in press) is more westerly than the predicted Elias motion, but has a magnitude that is too small to fit the data in most of the region. When assigned to the Peninsula block, many of the sites showed significant northerly residuals. Based on these tests, multiple upper blocks are required between the Bering Glacier and the Alaska Peninsula. A model with the Elias block extending to eastern Prince William Sound and the Peninsula block occupying the region to the west resulted in northerly and westerly trending residuals throughout the western Prince William Sound, Kenai Peninsula, and Kodiak Island regions. In addition, relative block motion between the Peninsula block and the Elias block caused significant (and unreasonably high) amounts of extension in eastern Prince William Sound. Estimating the motion of this region as a single block resulted in a poor fit to the data and a block motion that was higher and more westerly than the predictions of the Peninsula block.

After a number of tests, we concluded that in order to capture the motion exhibited in the data, several blocks are needed. The first block, termed the Prince William Sound block, extends from eastern Prince William Sound to the southern end of the Kenai Peninsula. The next block, the Kachemak block, extends from the southern end of the Kenai Peninsula to a point south of Kodiak Island. Further west, the Peninsula block as discussed above is assumed to be the upper plate block. For each of these blocks, the northern boundary is defined to be the Castle Mountain fault or a western extension of the Lake Clark fault. Once these blocks were defined, most of the data in the region were fit reasonable well, with the exception of sites along the trench side of Kodiak Island. These sites displayed residuals indicating a need for additional northwesterly motion. The trenchward side of Kodiak Island has a number of faults (e.g. *Carver et al.*, 2008) suggesting that there could be a crustal sliver moving relative to the rest of the Alaska forearc. Allowing sites in this area to be on a separate block resulted in block motion that was larger and more northerly than those of the Kachemak block. This provided a better fit to the data along the coast of Kodiak as well to the data remaining on the Kachemak block (the Kodiak data was forcing the block motion to have a larger magnitude).

Final Model Assembly

The final model assembly involved integration of the various pieces described above, making sure that all boundaries and definitions were consistent. Block angular velocities from such a joint model can differ from those of the regional or piecemeal models mainly because of elastic deformation effects that can extend over long distances. In addition, because all blocks must close, some degree of trial and error is required to find the proper block boundaries. For example, the definition of the Peninsula block as described above did not define where the eastern end of the block is located, and the final model turns out to be very sensitive to this definition.

Reconciling the northernmost parts of the models was fairly simple. The Kobuk fault was extended east to meet with the southern boundary of the North Coast block. Velocities on the Arctic and North Coast blocks show quite different trends, so a creeping boundary (which could represent distributed deformation; data sparseness prevents precise evaluation of the nature of any boundary) was placed to the west of the Richardson Mountains where seismicity indicates active deformation is occurring and near to a band of distributed seismicity in northeastern Alaska.

Merging the other western blocks with the other models proved more involved. Velocities in between the Denali and Kobuk faults in central Alaska, a region that includes the Fairbanks area, are very small and do not show trends similar to any of the surrounding blocks (Bering and Kuskokwim to the west and Northern Cordillera further east). Because of this, creeping boundaries (as above, data distribution does not allow precise definition of boundaries) were added to the west and east of this region, creating the Fairbanks block. This block encompasses the northeast trending Minto Flats, Fairbanks, and Salcha seismic zones (Ruppert et

al., 2008), so this area may be undergoing distributed deformation that cannot be fully explained by rigid boundaries. As described above, the region immediately south of the central Denali fault was divided into two blocks. The western of these blocks, termed the Southern Alaska block, could have reasonably been assumed to extend further west through the region bounded by the Castle Mountain/Lake Clark fault and the western extension of the Denali, the Farewell fault. However, predicted block motions for the Southern Alaska block in the region had orientations and magnitudes that did not provide a good match to the data. For this reason, we included a creeping boundary to define a western limit to the southern Alaska block and define the area to the west as the Naknek block.

The development of the block configuration south of the Castle Mountain and Lake Clark faults was discussed in a previous section.

Figure 9. Blocks used in the model. Dashed lines represent creeping faults whose boundaries may be uncertain or represent distributed deformation.

The final model block configuration is shown in Figure 9. Dashed lines represent creeping boundaries, where boundaries are uncertain because of data sparseness or because the model preferred a creeping fault over a locked fault. The final model faults that define these blocks are shown in Figure 10. Dashed lines are again creeping boundaries. Solid black lines are vertical or near vertical strike-slip faults, open teeth indicate blind thrusts, and solid teeth indicate thrust fault that daylight. Red outlines show extent of subducting Yakutat slab while orange outlines

show the Pacific slab. Numbers indicate coupling, with 1 being fully locked and 0 being fully creeping.

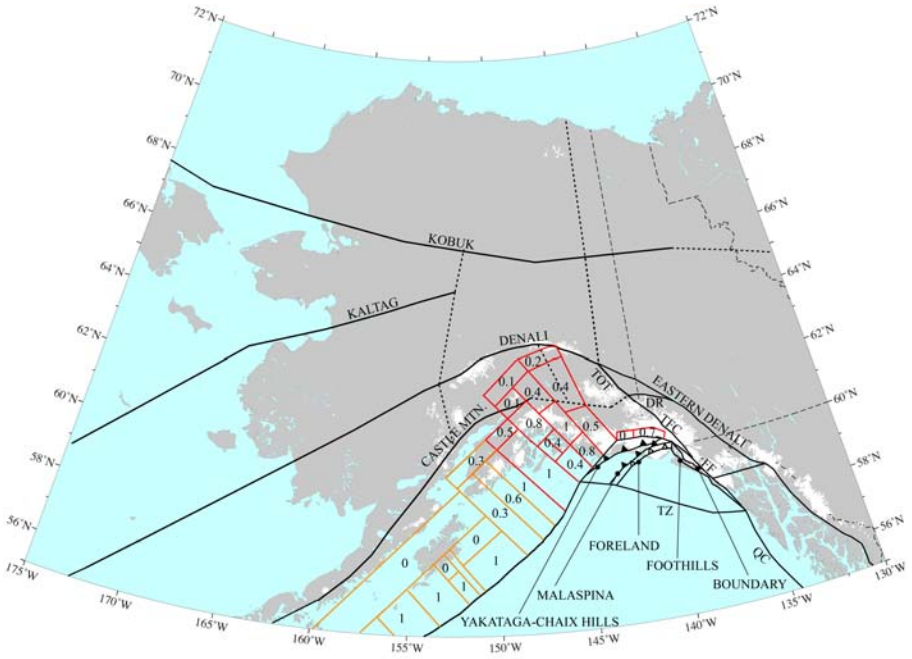

Figure 10. Faults used in model. Solid plain lines represent strike-slip faults, barbed lines represent thrust (open teeth denote buried thrust), red boxes represent subducting Yaktuat slab, and orange boxes represent subducting Pacific slab. Numbers indicate coupling coefficient on subduction planes.

Results

We inverted 671 data (east and north components of GPS velocities at 307 sites, X, Y, and Z components of the a priori angular velocity for the Pacific plate as estimated by GEODVEL (*Argus et al.*, 2010), and 54 slip constraints to estimate 72 model parameters (X, Y, and Z components of angular velocity for 24 blocks). We then transformed the estimated angular velocities from the XYZ coordinate system into the geographic coordinate system (latitude, longitude, and rotation rate) to present the block rotations in the familiar Euler pole format. Figure 11 and Table 1 show the Euler poles, rotation rates, and associated uncertainties for our final preferred model. Figure 12 displays the residuals, and Figure 13 the predicted linear surface block velocities.

As discussed in *Elliott et al*. (2010) and *Elliott et al.* (2013), small blocks at high latitudes have distorted uncertainty ellipsoids due to a large uncertainty in the local vertical component of the angular velocity and the nonlinear transformation between geographic and Cartesian coordinates. To compensate for this effect, we display a Monte Carlo sampling of the uncertainty regions with the poles in Figure 11 rather than approximating the uncertainty regions with the familiar 95% confidence ellipse. We took 2500 random samples of a zero-mean distribution with

a covariance equal to the angular velocity covariance, added each sample to our estimated angular velocities, computed the corresponding Euler pole, and the plotted the pole as a point on the map. The density of the points on the map corresponds to the probability distribution of the pole location. For blocks with large uncertainty regions for the poles, the predicted linear block velocities will still have small uncertainties because of the strong correlation between the pole location and angular speed.

Table 1. Block angular velocities estimated in this study. The pole latitude and logintude are given in decimal degrees, and the angular speed (rate) is given in degrees per million years. See Figure 11 for a graphical representation of pole uncertainties.

Block	Latitude (°N)	Longitude (°W)	Rate (deg/Myr)
Malaspina	60.40	-138.54	-13.79 ± 2.0
Icy Bay	64.43	-122.05	-1.71 ± 0.43
Elias	55.94	-155.44	0.71 ± 0.11
Northern Cordillera	52.08	-127.14	-0.15 ± 0.01
Yakutat	5.80	-25.19	-0.48 ± 0.01
Bering Def. Zone	57.63	-146.15	1.92 ± 0.60
Fairweather	55.39	-125.38	-0.34 ± 0.08
Baranof	38.34	-60.85	-0.04 ± 0.01
Nunatak	55.70	-149.61	3.53 ± 1.0
Foothills	44.96	-166.29	1.20 ± 0.23
Eastern Denali	61.73	-151.46	0.36 ± 0.14
PWS	54.52	-152.50	0.73 ± 0.13
Arctic	74.28	-111.05	0.08 ± 0.04
Bering Sea	11.93	-64.03	0.03 ± 0.01
Kuskokwim	55.33	116.28	-0.05 ± 0.02
Naknek	64.30	-165.02	-0.47 ± 0.07
Southern Alaska	58.67	-148.38	0.87 ± 0.13
Fairbanks	64.02	-147.82	-0.58 ± 0.10
Kodiak Sliver	69.74	-144.30	-0.52 ± 0.22
North Coast	61.75	-138.91	-0.20 ± 0.07
Wrangell	42.47	-169.75	0.15 ± 0.16
Eastern Alaska Range	63.37	-148.99	1.11 ± 1.2
Kachemak	64.30	-154.05	-0.83 ± 0.1
Peninsula	64.42	-175.57	-0.26 ± 0.10

The blocks with poles located furthest outside the area, including Kuskokwim, Bering Sea, and Arctic, display relatively uniform velocities across their blocks. However, most of the poles are located within or near the bounds of our study region. Poles located closer to their blocks, such as Southern Alaska and Fairbanks, generate velocities with more variations in magnitude or orientation across the block area.

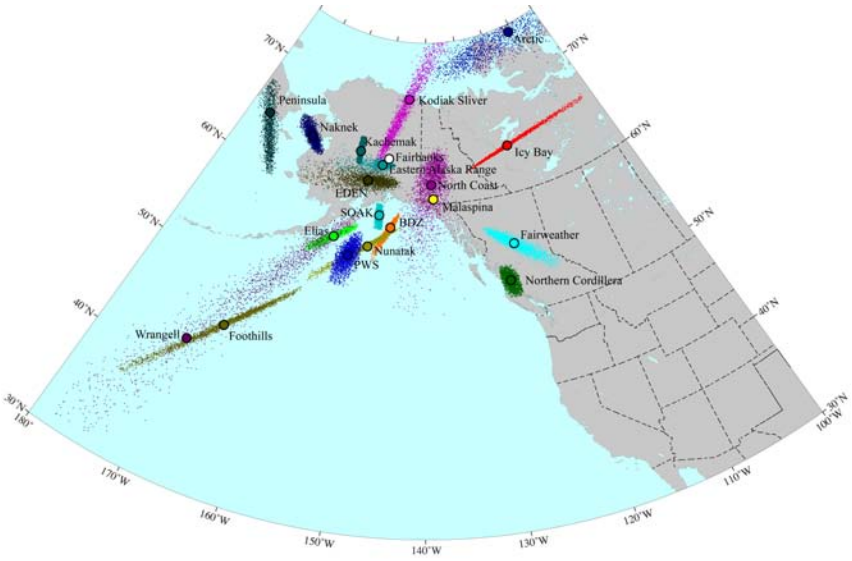

Figure 11. Euler pole locations for model blocks. Colored clouds represent 95% uncertainty regions for the poles. Poles not pictured as they are located farther from study region: Yakutat, Kuskokwim, and Bering Sea.

Predicted relative motions between neighboring blocks resolved onto the block-bounding faults are shown in Figure 14. The majority of the relative motion in the region is accommodated along what can be considered major boundary faults: the Fairweather-Queen Charlotte transform system, the series of closely spaced crustal thrust faults in the St. Elias, and the Alaska-Aleutian subduction zone. Smaller, but still quite significant, amounts of motion are accommodated on a number of structures away from the main boundary faults, including the Denali fault system, the Totschunda fault, a connector between the Fairweather and Totschunda faults, the Kobuk fault, and the Kaltag fault.

Our preferred block model provides a reasonable explanation for the observed GPS velocity field as shown by the data-model residual velocity plot in Figure 12. The reduced chi squared for the model is 4.2. While the residual velocities do not show much coherent spatial trend in any region, they do show a difference in magnitude between the regions close to the main plate boundaries and those in the far field. Blocks farther from the boundary, and in particular far from the influence of the Yakutat block, such as Arctic, North Coast, Bering Sea, Kuskokwim, Northern Cordillera, and Naknek, display very small residuals. Blocks closer to the main boundaries or the influence of the Yakutat block show larger magnitude residuals. This suggests that closer to the southern margin, the accommodation of strain may result in internal block deformation or diffuse deformation in addition to discrete block-like deformation. Alternatively, transient deformation that is not modeled well enough in our study may contribute to these residuals. In the far field, blocks appear to be well described by rigid rotations.

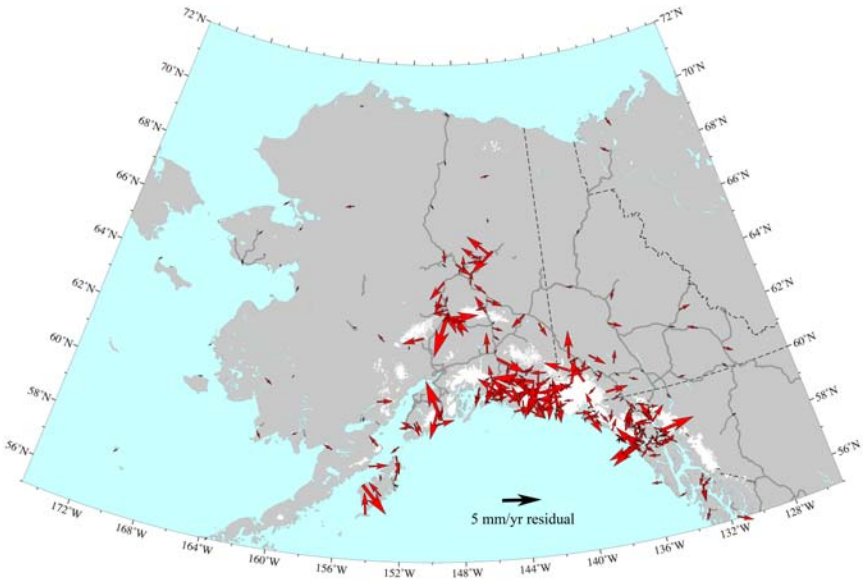

Figure 12. Data-model residuals for our preferred model. Data uncertainty ellipses have been omitted for clarity.

Tectonic and Hazard Interpretations

Large Scale Regional Tectonics

Previous large-scale models of Alaska tectonics (e.g. *Lahr and Plafker*, 1980; *Bird,* 1996) largely depended on sparse information and suggested that the region north of the Denali fault has little to no motion. More recent geodetic studies provided more detailed evaluations of deformation in western Alaska (e.g *Cross and Freymueller,* 2008), interior Alaska (e.g. *Fletcher*, 2002), southeast and southcentral Alaska (e.g *Elliott et al.*, 2010,2013), and the Alaska Peninsula (e.g. *Fournier and Freymueller*, 2007; *Cross and Freymueller*, 2008). Since these studies focused on subsets of Alaska, however, it was difficult to evaluate how processes in one region may influence deformation in another.

Our predicted block motion (Figure 13) shows a complex pattern of deformation. In southern Alaska, the deformation bears similarities to patterns observed in the Himalaya due to the collision of India and Eurasia (e.g. *Meade*, 2007), although on a much smaller scale. Immediately inboard of the Yakutat collision, northward velocities extend into the Yukon and eastern Alaska. To the east, a clockwise rotation of velocities extends deformation into the Mackenzie Mountains. To the west-northwest (subparallel to the direction of Yakutat motion), a larger scale counterclockwise rotation suggests lateral extrusion of material along strike-slip faults inboard of the megathrust.

There is an ongoing debate about the nature of the interaction between the Yakutat block and southern Alaska. One end-member model suggests that the Yakutat block acts as an indentor, with the sedimentary cover of the Yakutat block traveling northwestward coupled to the basement. The collision would

deform the original Yakutat-southern Alaska suture into an oroclinal bend as the sedimentary cover is stripped off to form a fold-and-thrust belt (e.g. *Pavlis et al.*, 2004; *McCalpin et al.,* 2011). Left lateral shear would occur at the western end of the St. Elias orogen while dextral shear would dominate at the eastern end. The other end-member model postulates that the Yakutat collision results in something akin to a train wreck, where the sedimentary cover would decouple from the Yakutat basement, rotate counterclockwise, and extrude along the megathrust (*McCalpin et al.*, 2011). Dextral shear would dominate the region. Our results show that a model between the two end-members is required. Inboard of the Yakutat collision, the pattern of the deformation into the Yukon and the fold-and-thrust belt along the southern Alaska coast resemble the effects of an indentor. Although there is some indication of left-lateral shear around the Bering Deformation Zone, eastern Prince William Sound, and the Kenai Peninsula, the latter two instances are due to coupling variations along the megathrust, making the relationship to a possible orogen outlet complex. Inboard of the fold-and-thrust belt, the number of counterclockwise rotating blocks south of the Denali fault and along the forearc of the megathrust strongly resemble the train wreck model. Taking the region as a whole, dextral shear dominates.

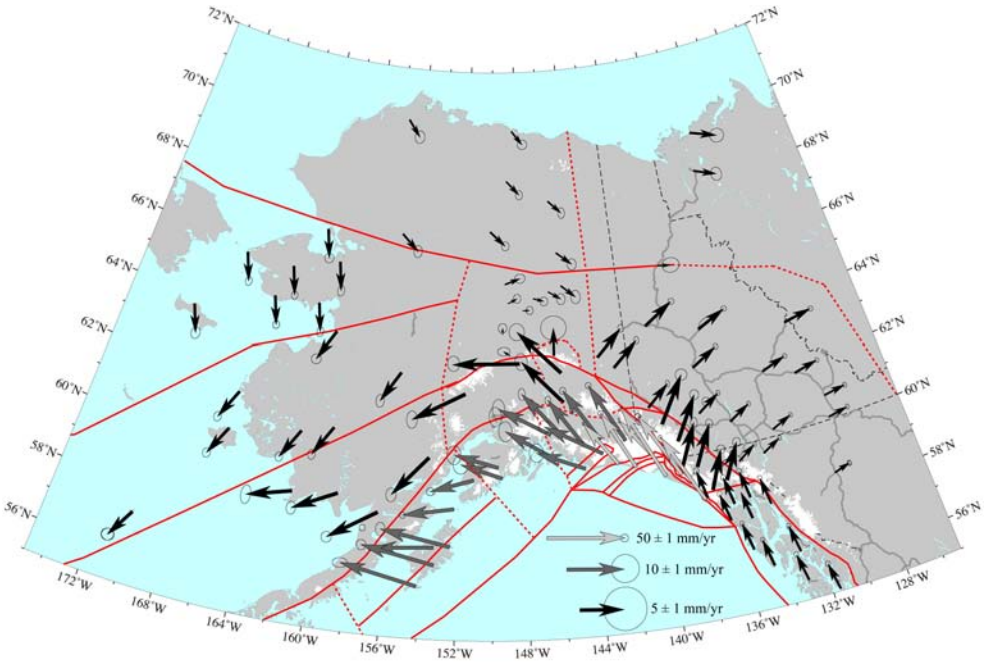

Figure 13. Model block velocity predictions. The predictions are for block motion only and do not include effects of elastic strain accumulation. Note different scales for different colored vectors.

Bird (1996) suggested that the fold-and-thrust system inboard of the Yakutat collision and trench-parallel motion along the forearc were isolated from each other and that no material was escaping to the west. Our results show a clear continuation of the deformation pattern from the fold-and-thrust belt into the forearc as well as westward lateral excape. Rather than separate systems, tectonic

processes in the region seem to be strong links to the collision and subduction of the Yakutat block.

It is important to note that the strike-slip faults in western Alaska have dextral shear in our model. This is in contrast to the estimates of relative motion between the Pacific and North American plates, which would predict left-lateral oblique shear on the faults. Reporting on evidence of recent dextral transpression on structures including the Castle Mountain fault, *Haeussler et al.* (2000) suggested that the dextral motion was driven by the Yakutat collision and caused the lateral escape of part of the accretionary complex to the west. Our results support this idea and go further to suggest more than part of the accretionary complex is undergoing lateral escape.

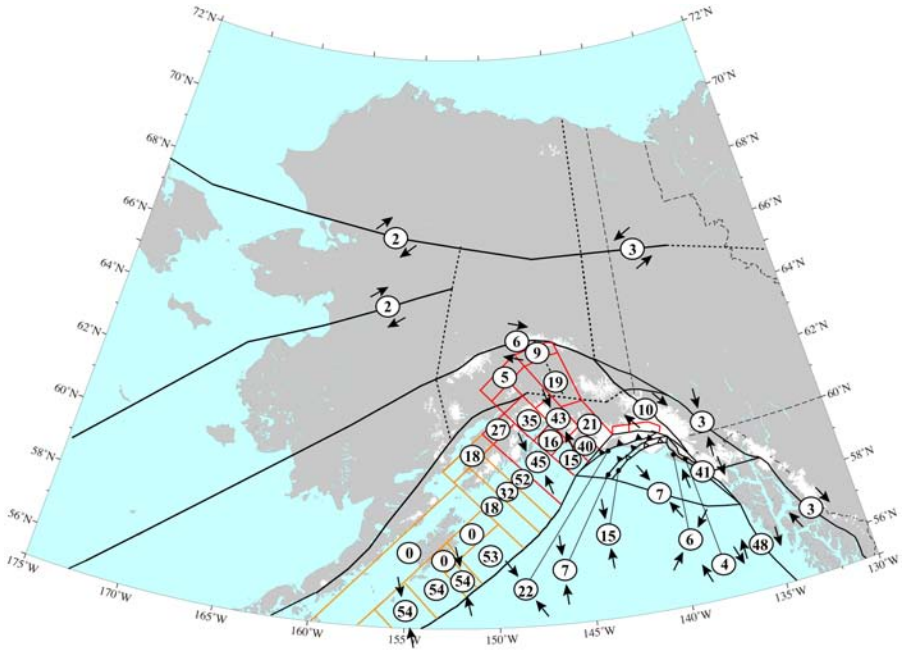

Figure 14. Relative motions between neighboring blocks resolved onto the assumed block-bounding faults. Numbers in circles are the magnitudes of the relative motion in mm/yr. Arrows show direction of relative motion. Coupling coefficients have been applied.

North of the Denali fault, there is a significant change in the deformation field. Instead of northerly or westerly motions, the velocity field displays various degrees of southerly motion. Part of this motion may be linked to larger scale plate motions extending into far east Russia (e.g. *Mackey et al*., 1997), part may be associated with mantle flow around the edge of the shallowly subducting Yaktuat slab (e.g. *Finzel et al.* , 2011), and part may have some relation to the tectonics of the opening of the Arctic Ocean basin. Further work is required to distinguish between various processes.

Figure 14 shows relative motion between adjacent blocks for our preferred model, resolved onto the block bounding faults. These rates may be considered as geodetic estimates of the fault slip rates, although it must be kept in mind that some of the boundaries are approximate and may represent the sum of several faults. Where the fault geometry has been simplified, the strike-slip and dip-slip components need to be used with care. The majority of the relative motion is accommodated along the major boundary faults (the Fairweather-Queen Charlotte Transform system, the St. Elias fold-and-thrust belt, and the Alaska megathrust), but significant motion also occurs away from the main boundary. In general, southeast Alaska is dominated by dextral motion, the more western parts of southern Alaska are dominated by oblique convergence, and the regions inboard of the main boundary is dominated by dextral motion.

Slip Rates and Seismic Hazard

For some of the faults, we present updated geometries and slip rates. For other faults, these results serve as the first geodetically derived estimate of slip. In southeast Alaska and the St. Elias and Chugach ranges, slip rates on faults are similar to those reported in *Elliott et al* (2013) and *Elliott et al*. (2010), although combining the models did cause a few changes as noted below. The uppermost Fairweather fault, which is closest to the Yakutat collisional front, has an estimated 35 ± 0.8 mm/yr of right-lateral strike-slip and 9 ± 4 mm/yr of convergence. The central Fairweather has a higher strike-slip rate of 45 ± 0.6 mm/yr of dextral motion and a lower convergence rate of 6 ± 0.4 mm/yr. As this section of the fault approaches the offshore junction with the Queen Charlotte fault, the estimated convergence across the fault increases to ~10 mm/yr. Along the Queen Charlotte, which is entirely offshore, the model estimates an average of 45 ± 0.6 mm/yr of right-lateral slip. Fault normal motion increases from north to south, from ~10 mm/yr of convergence near the junction with the Fairweather to nearly 18 mm/yr of convergence outboard of Haida Gwaii, the location of a M7.5 thrust event in 2012.

Outboard of the Fairweather fault, our model predicts an average of 3 ± 1 mm/yr of right-lateral strike-slip motion and 1 ± 1 mm/yr of extension along the Boundary fault. The fault normal motion changes from convergence at the north end of the fault to extension at the south end due to changes in the orientation of the model fault geometry. Further west, along the Foothills thrust, the model puts an average of 3 ± 0.7 mm/yr of right-lateral strike-slip and 4.5 ± 0.7 mm/yr of convergence on the fault. As noted in *Elliott et al.* (2010), these faults may have been involved in the 1899 earthquake sequence that occurred in the vicinity of Yakutat Bay.

Due to lack of geodetic data constraints, the Totschunda and upper Eastern Denali faults were constrained to have slip rates compatible with geologic estimates. The model predicts averages of 2.7 ± 0.3 mm/yr of right-lateral motion and 1 ± 0.7 mm/y of extension along the Totschunda. This rate is lower than the geologic estimate of ~5 mm/yr (*Seitz et al*., 2008), but the geodetic rates may change with

additional data. Along the upper Eastern Denali fault, the model estimates an average of 4 ± 0.4 mm/yr of right-lateral motion and 2 ± 0.6 mm/yr of extension.

Further south, the Duke River fault displays an estimated 2 ± 0.4 mm/yr of left-lateral strike-slip motion and 2 ± 0.6 mm/yr of convergence across the fault. Between the Duke River fault and Lynn Canal, the central segment (the Dalton Strand) of the Eastern Denali fault is predicted to have an average of 2 ± 0.2 mm/yr of right-lateral strike-slip motion and 2 ± 0.2 mm/yr of convergence. This dextral transpression is due to the rotation of our model Fairweather block into the Northern Cordillera and is consistent with a sequence of closely spaced M6 earthquakes that occurred in June 2017 near the junction of the Duke River fault and the Eastern Denali fault. The first event had a dominantly thrust mechanism while the second showed strike-slip motion, suggesting possible slip partitioning of the relative block motion. South of the Eastern Denali fault, our block model includes the Coast Shear zone. The model estimates an average of 3 ± 2 mm/yr of right-lateral strike-slip and 1 ± 2 mm/yr of extension along the fault. This may represent regional shear rather than motion along a discrete structure.

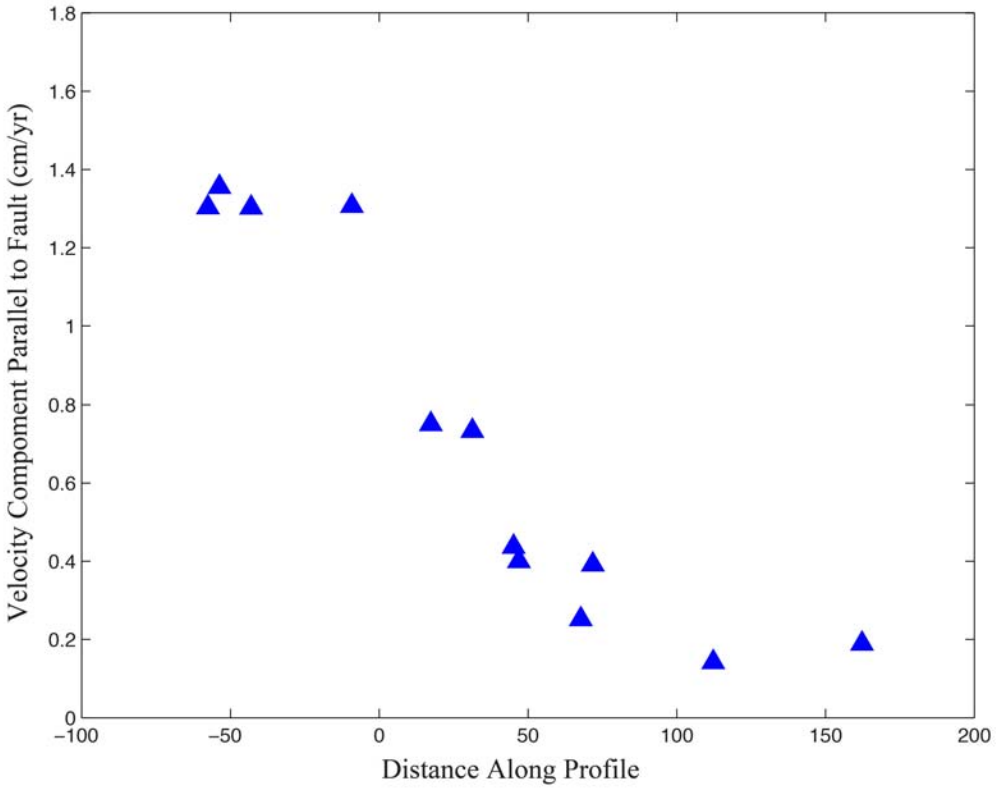

Figure 15. Velocities parallel to the inferred Connector Fault, along a fault-normal profile. The fault location is at distance zero. The data clearly show ~11 mm/yr of strike-slip motion. The profile is asymmetric about the inferred fault location, which could indicate a mislocated fault, a NE-dipping fault, or a contrast in elastic properties across the fault.

One major difference with the previous southeast Alaska model of *Elliott et al.* (2010) concerns the postulated Totschunda-Fairweather Connector fault. As discussed in that paper, previous regional geologic studies (e.g. *Richter and Matson*, 1971; *Lahr and Plafker*, 1980) suggested a possible structural connection between the Totschunda and Fairweather faults that might lie along a series of NNW-ESE trending linear valleys. The 2010 model included the postulated connector fault but did not have robust data constraints in the region, leading to an estimate of several mm/yr of extension across the fault. *Marechal et al*. (2015), using new GPS data from the Yukon and a subset of data from *Elliott et al*. (2013) suggested that no discrete structure was required and that distributed deformation or continuum deformation could explain the observed velocity pattern. Using the full available data set on either side of the proposed connector, we find a different pattern. The velocities (Figure 15) show a clear change in the vicinity of the Connector fault consistent with right-lateral motion. The block model predicts an average of 9 city pattern. Usght-lateral motion and 2 ± 0.4 mm/yr of extension along the fault. This rate of dextral motion would be consistent with a connector fault between the Fairweather system and the slower Denali-Totschunda system. This result also suggests that a major change may be needed to the current seismic hazard maps, which assume motion transfers from the Totschunda to the Duke River and then the Eastern Denali faults. *Lahr and Plafker* (1980) suggested that the tectonic system is evolving so that relative plate motion is transferring west from the Duke River-Eastern Denali system to a Totschunda-Connector-Fairweather system. Our results support that hypothesis.

Further west, the closely spaced structures in the St. Elias fold-and-thrust belt accommodate the majority of relative motion in the region, although the distribution of the motion between the faults is different than that in Elliott et al. (2013). This is largely due to the merger of the southeast Alaska and St. Elias model, which connects the upper Fairweather, Boundary, and Foothills faults with the thrust belt. The outermost thrust, the Foreland Fault zone, is modeled as a buried thrust that links to a developing fault offshore (*Elliott et al.*, 2013). Our model predicts an average of 2.8 the St. Elias follateral strike-slip and 20 ± 2 mm/yr of convergence along the structure. It should be noted that part of the model planes that make up this fault zone are offshore and east of data constraints. If an average is taken only over fault segments constrained well by GPS data, the slip averages are 0.3 ± 0.8 mm/yr of right-lateral strike slip and 19 ± 2 mm/yr of convergence. These rates are higher than the rates predicted by the model of *Elliott et al*. (2013). The Malaspina fault has an estimated average of 3 ± 0.8 mm/yr left-lateral strike-slip and 4.4 ± 2 mm/yr of convergence, although slip varies along the fault. Immediately offshore, the model predicts ~ 7 mm/yr of left-lateral slip and ~15 mm/yr of reverse motion, although this segment has a lower degree of coupling. Through the main part of Icy Bay, the fault appears to be fully creeping. Further north, along the Samovar Hills, the model estimates 6 ± 0.8 mm/yr of left-lateral slip and 3.9 ± 1.5 mm/yr of reverse slip. The sense of slip is the same as that discussed in *Elliott et al*. (2013), but the magnitude of dip-slip is lower. Further east, the current model estimates 2.3 and 4.4 ± 2 mm/yr of convergence, although slip varies along the

fault. Immediately offshore, the model predicweather, but this region has few data contraints. The Yakataga-Chaix Hills fault, which is a composite of several closely spaced thrust faults (see *Elliott et al.* 2013 for discussion) has estimated average rates of 10.8 ataga-Chaix Hills fault, which is a composite of s± 0.5 mm/yr of reverse slip. These predictions are very similar to those in the previous study.

Along the central Denali fault, which includes the crossings of the Parks and Richardson Highways and thus multiple GPS data profiles, our model predicts an average of ~ 6 mm/yr of right-lateral strike-slip. The area west of the Richardson Highway shows slip of 7 ± 0.4 mm/yr right-lateral strike-slip and 0.3 ± 0.5 mm/yr of extension along the fault. The area surrounding the Richardson Highway and the area further east to the junction with the Totschunda fault show average slip rates of 5.4 ± 0.8 mm/yr right-lateral strike-slip and 1.3 ± 1.7 mm/yr of extension. These rates are consistent with previous geodetic estimates (e.g. *Fletcher*, 2002; *Freymueller et al*., 2008), but are significantly lower than geologic estimates of late Quaternary slip derived from cosmogenic surface exposure data of offset surfaces along the fault (*Hauessler et al*., 2017). Those estimates suggest the central Denali may have dextral slip of as much as ~13 mm/yr. As *Hauessler et al*. (2017) points out, all of the geodetically derived slip estimates rely on data collected prior to the 2002 M7.9 Denali Fault earthquake. That holds true for the present model as well, which results in higher data uncertainties and a limitation in the spatial coverage. This limitation could influence the slip estimates and additional data in the future will be needed to evaluate whether the geodetic estimates reflect robust estimates of slip. If they do, this will require further reconciliation with geologic estimates.

The subduction interface in our preferred model extends further east and north than previous models (Figure 14). Along the easternmost and northern segments, coupling in less than in the segments nearer the coast. Where they overlap, the general coupling pattern resembles that of several previous geodetic models (e.g. *Zweck et al*, 2002; *Suito and Freymueller*, 2009). The interface beneath Prince William Sound, including the hypocentral region of the 1964 earthquake, appears to be strongly locked. A region of low coupling occurs beneath the western Kenai Peninsula. Strong coupling marks the seaward side of Kodiak Island while the landward side of the island appears to be creeping. Farther east, very small partially coupled segments lie north of the fold-and-thrust belt. This partially coupled region corresponds to the region that may have been responsible for the M7.8 1979 St. Elias earthquake (*Estabrook et al.*, 1988). Beneath the crustal faults of the fold-and-thrust belt, the decollement appears to be creeping. Allowing partial coupling along this interface increased the misfit to the data; the high strain gradient observed in the data is best described with crustal thrust faults. *Shennan et al* (2009) presented evidence that past great earthquakes have ruptured larger areas than that ruptured during 1964 and involved faults as far east as Icy Bay. If the decollement beneath the fold-and-thrust belt is creeping, this implies that events on the megathrust may load the crustal thrust faults and promote failure.

This study presents the first geodetically derived estimates of slip rates along several faults. In western Alaska, the western extension of the Denali fault has an average estimated slip of 0.5 ± 0.4 mm/yr of right-lateral strike-slip and 0.2 ± 0.5 mm/yr of extension. The fault displays slightly more transpression at the western end and slightly more transtension at the eastern limit. These low rates of motion are consistent with previous geologic studies (e.g. *Matmon et al*., 2006) that suggested evidence for the westward decrease in slip rates along the Denali system. Motion west of the central Denali fault is likely accommodate through more diffuse deformation, potentially within the north-south trending Revelation Mountains which coincides with our model boundary between the Southern Alaska block and the Naknek block. Further north, our model Kaltag fault has an estimated 2.3 ± 0.3 mm/yr of dextral motion and 0.8 ± 0.4 mm/yr of convergence. The model predicts 1.3 ± 0.3 mm/yr of dextral motion and 1.4 ± 0.5 mm/yr of extension along the Kobuk fault. This result is consistent with a series of earthquakes in 2014. Three M5+ earthquakes, two with normal fault mechanisms and one with a strike-slip mechanism, occurred near Noatak, Alaska north of the Kobuk fault.

Further south, our model predicts an average of 0.4 the westward decrease in slip rates along the Denali system. Motion west of the central Denali fault is likely acark faults. The model slip becomes more transtensional towards the east and more transpressional to the west. This is different from geologic studies of the Castle Mountain fault, which suggested that up to 3 mm/yr of right-lateral strike-slip may occur along the fault (*Willis et al*., 2007) and that thrusting has occurred during past events (*Haeussler et al*, 2002). It should be noted, however, that data is sparse around the Castle Mountain fault. Some sites in the region were exclude due to possible contamination from transient events and the overall number of sites was low to begin with. Densifying the network of GPS sites in this region should be a target for future work.

Unsolved problems and Directions for future work

As mentioned above, further work is required to determine which processes are responsible for the southerly motions in northern and northwestern Alaska. How this deformation regime transitions into the Richardson and Mackenzie Mountain regions in northwestern Canada is currently poorly constrained due to very sparse data. Also uncertain is the nature of deformation in the Fairbanks region. In our model, it appears to behave a sort of hinge line between the convergent boundary to the south and the southward motion to the north. However, our model also implies that there is some transfer of slip inboard from the Denali fault to the Kaltag fault, and the geometry and structures involved in that are not clear in the present data. Earthquake data support the existence of left-lateral, northeasterly trending shear zones in the region, but we could not resolve any significant deformation associated with these zones. The seaward extensions of the block boundaries along extensions of the Kobuk, Kaltag, and Farewell faults is speculative and not well constrained. Future work should integrate this model with

constaints from seismicity in the Bering Sea and Russian Far East, which may help in assigning the most realistic block boundaries.

South of the Denali fault, the exact geometry of the easternmost Alaska subduction zone is a matter of debate. A major question remains as to whether there is a continuous interface underneath the Wrangell Mountains or whether there may instead be a slab edge in the vicinity. Slip behavior along this section of the interface is also uncertain, although we do infer an edge to the locked part of the subduction interface. Whether this represents a true slab edge or simply an along-strike change in the slip behavior cannot be determined yet. Current instrumentation does not allow for the detection of transient slip events that may be associated with the observed tremor of Wech (2016). Motion of the northernmost Eastern Denali fault is poorly constrained due to sparse data. The limitation of using only pre-2002 data to determine Denali fault slip rates could bias results, for example if a transient event such as one of the large slow slip events in Cook Inlet substantially affects these sites. The Castle Mountain fault does not have many near-field data constraints, resulting in a slip estimate that may not be robust.

Many of these uncertainties arise from the sparseness of available data. Some of this sparseness is a result of lack of sites while some is caused by the need to exclude data from sites contaminated by non-long-term tectonic motion. The lack of a robust postseismic model for the 2002 Denali Earthquake severely limits the use of data in southcentral and interior Alaska. No postseismic model yet exists for the Haida Gwaii and Craig, Alaska events, although this has a smaller impact on the model. The detailed time dependence of the older slow-slip events in Cook Inlet have proven difficult to model, mainly because of a lack of continuous data, resulting in the exclusion of a number of sites in the region.

Several recent and ongoing NSF-funded projects will bring in new data relevant to these questions. An Earthscope project in the Northern Cordillera of Canada (led by PI Freymueller) will help resolve the nature of strain transfer across the Yukon into the MacKenzie Mountains. Two separate Earthscope projects will examine deformation (led by PI Elliott) and seismicity and structure (led by Doug Christensen at UAF and Geoff Abers at Cornell) in southcentral Alaska to better constrain the geometry and slip behavior of the easternmost Alaska subduction zone.

As this new data is available and as refinements to models transient and non-tectonic motions are made, the model presented here can be expanded and refine in terms of data. In the nearer future, this model will be merged with subduction strain models for the Alaska Peninsula (Li and Freymueller, in press) and the Aleutian arc (Cross and Freymueller, 2008), which may help answer some questions about how the strike-slip faults in western Alaska may terminate. Another major future goal is to incorporate distributed or internal block deformation. Initial experiments into this have been performed, but the current sparseness of data in key areas have resulted in unreliable results. As more data becomes available, estimates of internal strain will become more robust.

Personnel

The main portion of the work on this project was carried out by the two PIs, Elliott and Freymueller, with contributions from several graduate students. At the University of Alaska Fairbanks, master's student Kimber deGrandpre compiled information for northern and western Alaska, and helped with the development of the initial test block models for that region. Ph. D. student Shanshan Li worked on models for the Alaska Peninsula and Aleutian arc.

Publications Resulting from this Work

Li, S., and J. T. Freymueller (2018), Spatial Variation of slip behavior beneath the Alaska Peninsula along Alaska-Aleutian Subduction Zone, *Geophysical Research Letters*, 2017GL076761.

Another paper is in preparation.

References

Agnew DC (1997) NLOADF: a program for computing ocean-tide loading. J Geophys Res 102:5109–5110

Argus, D. F., R. G. Gordon, M. B. Heflin, C. Ma, R. J. Eanes, P. Willis, W. R. Peltier, and S. E. Owen (2010), The angular velocities of the plates and the velocity of Earth's centre from space geodesy, Geophys. J. Int., 180(3), 913–960.

Bird, P. (1996), Computer simulations of Alaskan neotectonics, *Tectonics*, 15(2), 225–236, doi:10.1029/95TC02426.

Carver, G. , Sauber, J. , Lettis, W. , Witter, R. and Whitney, B. (2013). Active Faults on Northeastern Kodiak Island, Alaska. In Active Tectonics and Seismic Potential of Alaska (eds J. T. Freymueller, P. J. Haeussler, R. L. Wesson and G. Ekström). doi:10.1029/179GM09

Cross, R. S., and J. T. Freymueller (2008), Evidence for and implications of a Bering plate based on geodetic measurements from the Aleutians and western Alaska, J. Geophys. Res., 113, B07405, doi:10.1029/2007JB005136

Elliott, J. L., C. F. Larsen, J. T. Freymueller, and R. J. Motyka (2010), Tectonic block motion and glacial isostatic adjustment in southeast Alaska and adjacent Canada constrained by GPS measurements, *J. Geophys. Res.*, 115, B09407, doi:10.1029/2009JB007139.

Elliott, J., J. T. Freymueller, *and* C. F. Larsen *(*2013*),* Active tectonics of the St. Elias orogen, Alaska, observed with GPS measurements*, J. Geophys. Res. Solid Earth,* 118*,* 5625–5642*, doi:*10.1002/jgrb.50341.

Elliott, J., J. T. Freymueller, and C. F. Larsen (2013), Active tectonics of the St. Elias orogen, Alaska, observed with GPS measurements, *J. Geophys. Res. Solid Earth*, 118, 5625–5642, doi:10.1002/jgrb.50341.

Enkelmann, E., P. O. Koons, T. L. Pavlis, B. Hallet, A. Barker, J. Elliott, J. I. Garver, S. P. S. Gulick, R. M. Headley, G. L. Pavlis, et al. (2015), Cooperation among tectonic and surface processes in the St. Elias Range, Earth's highest coastal mountains, *Geophys. Res. Lett.*, 42, 5838–5846, doi:10.1002/2015GL064727.

Estabrook, C. H., J. L. Nabelek, and A. L. Lerner-Lam (1992), Tectonic model of the Pacific plate boundary in the Gulf of Alaska from broadband analysis of the 1979 St. Elias, Alaska, earthquake and its aftershocks, J. Geophys. Res., 97, 6587–6612.

E.S. Finzel, L.M. Flesch, K.D. Ridgway; Kinematics of a diffuse North America–Pacific–Bering plate boundary in Alaska and western Canada. *Geology* ; 39 (9): 835–838. doi: https://doi.org/10.1130/G32271.1

Fletcher, H. J., J. Beavan, J. Freymueller, and L. Gilbert, High interseismic coupling of the Alaska subduction zone SW of Kodiak island inferred from GPS data, *Geophys. Res. Lett.*, 28, 443-446, 2001.

Fletcher, H. J., Crustal Deformation in Alaska Measured using the Global Positioning System, Ph.D. thesis, University of Alaska Fairbanks, 135pp., 2002.

Fournier, T. J., and J. T. Freymueller (2007), Transition from locked to creeping subduction in the Shumagin region, Alaska, Geophys. Res. Lett., 34, L06303, doi:10.1029/2006GL029073

Freymueller, J.T., H. Woodard, S. Cohen, R. Cross, J. Elliott, C. Larsen, S. Hreinsdottir, C. Zweck (2008), Active deformation processes in Alaska, based on 15 years of GPS measurements, in *Active Tectonics and Seismic Potential of Alaska,* AGU Geophysical Monograph, 179, J.T. Freymueller, P.J. Haeussler, R. Wesson, and G. Ekstrom, eds., pp. 1-42, AGU, Washington, D.C.

Freymueller, J., Seasonal position variations and regional reference frame realization, in H. Drewes (ed.), *Geodetic Reference Frames*, International Association of Geodesy Symposia 134, pp. 191-196, Springer Verlag, doi:10.1007/978-3-642-00860-3_30, 2009.

Fu, Y., J. T. Freymueller, and T. van Dam, The effect of using inconsistent ocean tidal loading models on GPS coordinate solutions, *J. Geod.*, 86(6), 409-421, doi:10.1007/s00190-011-0528-1, 2011

Fu, Y., and J. T. Freymueller (2012), Seasonal and Long-term Vertical Deformation in the Nepal Himalaya Constrained by GPS and GRACE Measurements, *J. Geophys. Res.*, 117, B03407, doi:10.1029/2011JB008925.

Haeussler, P. J., R. L. Bruhn, and T. L. Pratt (2000), Potential seismic hazards and tectonics of the upper Cook Inlet basin, Alaska, based on analysis of Pliocene and younger deformation, *Geo. Soc. Am. Bull., 112*, 1414-1429.

Haeussler, P. J., T. C. Best, and C. F. Waythomas (2002), Paleoseismology at high latitudes: Seismic disturbance of upper Quaternary deposits along the Castle Mountain fault near Houston, Alaska, GSA Bulletin (2002) 114 (10): 1296-1310, DOI: https://doi.org/10.1130/0016-7606.

Haeussler, P. J., A. Matmon, D. P. Schwartz, G. G. Seitz (2017), Neotectonics of interior Alaska and the late Quaternary slip rate along the Denali fault system. *Geosphere* ; 13 (5): 1445–1463. doi: https://doi.org/10.1130/GES01447.1

Hu. Y., and J. T. Freymueller (in prep), Geodetic Observations of Glacial Isostatic Adjustment in Southeast Alaska and its Implication of Earth Rheology, to be submitted to *Journal of Geophysical Research*.

Kim, Y., G. A. Abers, J. Li, D. Christensen, J. Calkins, and S. Rondenay (2014), Alaska Megathrust 2: Imaging the megathrust zone and Yakutat/Pacific plate interface in the Alaska subduction zone, *J. Geophys. Res. Solid Earth*, 119, 1924–1941, doi:10.1002/2013JB010581.

Koehler, R.D., 2013, Quaternary Faults and Folds (QFF): Alaska Division of Geological & Geophysical Surveys Digital Data Series 3, http://doi.org/10.14509/qff. http://doi.org/10.14509/24956.

Lahr, J. C., and G. Plafker (1980), Holocene Pacific-North American plate interaction in southern Alaska: Implications for the Yakataga seismic gap, *Geology, 8*, 483-486.

Larsen, C. F., R. J. Motyka, J. T. Freymueller, K. A. Echelmeyer, and E. R. Ivins, Rapid viscoelastic uplift in southeast Alaska caused by post-Little Ice Age glacial retreat, *Earth Planet. Sci. Lett.*, 237, 548-560, 2005

Li, S., J. Freymueller, and R. McCaffrey (2016), Slow slip events and time-dependent variations in locking beneath Lower Cook Inlet of the Alaska-Aleutian subduction zone, J. Geophys. Res. Solid Earth, 121, doi:10.1002/2015JB012491

Li, S., and J. T. Freymueller (2018), Spatial Variation of slip behavior beneath the Alaska Peninsula along Alaska-Aleutian Subduction Zone, *Geophysical Research Letters*, 2017GL076761.

Mackey, K.G., Fujita, K., Gunbina, L.V., Kovalev, V.N., Imaev, V.S., Kozmin, B.M., and Imaeva, L.P., 1997, Seismicity of the Bering Strait region: Evidence for a Bering block: Geology, v. 25, p. 979–982, doi:10.1130/00917613(1997)025<0979:SOTBSR>2.3.CO;2.

Marechal, A., S. Mazzotti, J. L. Elliott, J. T. Freymueller, and M. Schmidt (2015), Indentor-corner tectonics in the Yakutat-St. Elias collision constrained by GPS, J. Geophys. Res. Solid Earth, 120, doi:10.1002/2014JB011842.

Matmon, A., Schwartz, D. P., Haeussler, P. J., Finkel, R., Lienkaemper, J. J., Stenner, H. D., & Dawson, T. E. (2006). Denali fault slip rates and Holocene‐late Pleistocene kinematics of central Alaska. Geology , 34(8), 645-648.

McCalpin, J. P., R. L. Bruhn, T. L. Pavlis, F. Gutierrez, J. Gutierrez, and P. Lucha (2011), Antislope scarps, gravitational spreading, and tectonic faulting in the western Yakutat microplate, south coastal Alaska, Geosphere, 7, 1143–1158, doi:10.1130/GES00594.1.

Meade, B. (2007), Present-day kinematics at the India-Asia collision zone: Geology , v. 35, p. 81–84, doi: 10.1130/G22924A.1, 2007.

Meade, B. J., & Loveless, J. P. (2009). Block modeling with connected fault-network geometries and a linear elastic coupling estimator in spherical coordinates. In *Bulletin of the Seismological Society of America* (6th ed., Vol. 99, pp. 3124-3139).

Pavlis, T. L., C. Picornell, and L. Serpa (2004), Tectonic Processes During Oblique Collision: Insights from the St. Elias Orogen, Northern American Cordillera, *Tectonics, 23*, TC3001, doi:10.1029/2003TC001557.

Richter, D. H., and N. A. Matson (1971), Quaternary faulting in the eastern Alaska Range, Geol. Soc. Am. Bull., 82, 1529–1540.

Ruppert, N. A., K. D. Ridgway, J. T. Freymueller, R. S. Cross, and R. A. Hansen (2008), Active Tectonics of Interior Alaska: A Synthesis of Seismic, GPS and Geomorphic Studies, in *Active Tectonics and Seismic Potential of Alaska,* AGU Geophysical Monograph, 179, J.T. Freymueller, P.J. Haeussler, R. Wesson, and G. Ekstrom, eds., pp. 109-133, AGU, Washington, D.C.

Seitz, G. J., P. J. Haeussler, A. J. Crone, P. Lipovsky, and D. P. Schwartz (2008), Eastern Denali fault slip rate and paleoseismic history, Kluane Lake area Yukon Territory, Canada, Eos Trans. AGU, 89(53), Fall Meet. Suppl., Abstract T53B–1947.

Shennan, I., R. Bruhn, and G. Plafker (2009), Multi-segment earthquakes and tsunami potential of the Aleutian megathrust, Quat. Sci. Rev., 28, 7–13.

Suito, H., and J. T. Freymueller, A viscoelastic and afterslip postseismic deformation model for the 1964 Alaska earthquake, *J. Geophys. Res.*, doi:10.1029/ 2008JB005954, 2009.

Willis, J. B., P. J. Haeussler, R. L. Bruhn, G. C. Willis (2007), Holocene Slip Rate for the Western Segment of the Castle Mountain Fault, Alaska. *Bulletin of the Seismological Society of America* ; 97 (3): 1019–1024. doi: https://doi.org/10.1785/0120060109

Zou, R., J. T. Freymueller, K. Ding, S. Yang, *and* Q. Wang *(*2014*),* Evaluating seasonal loading models and their impact on global and regional reference frame alignment*, J. Geophys. Res. Solid Earth,* 119*, doi:*10.1002/2013JB010186.

Zweck, C., J. T. Freymueller, and S. C. Cohen, The 1964 Great Alaska Earthquake: Present Day and Cumulative Postseismic Deformation in the Western Kenai Peninsula, *PEPI*, 132, 5-20, 2002.

Appendices

Velocity field

The velocity data are given in separate files, which are more useful than embedding them into a giant table in the PDF. The files are contained in a zip file called "Velocities.zip". That folder contains 6 files.

The following 4 files give the velocities in ITRF2008 and relative to North America, in a simple format called "GPS3D". The file used for all further work is Alaska-seasonal-NOAM.gps3d.

Alaska-ITRF.gps3d
Alaska-NOAM.gps3d
Alaska-seasonal-ITRF.gps3d
Alaska-seasonal-NOAM.gps3d

The file has 10 fields separated by whitespace:

1. Site name (string)
2. Longitude, decimal degrees (on 0-360)
3. Latitude, decimal degrees
4. Elevation, meters
5. East velocity, cm/yr
6. North velocity, cm/yr
7. Vertical velocity, cm/yr
8. East velocity uncertainty, cm/yr
9. North velocity uncertainty, cm/yr
10. Vertical velocity uncertainty, cm/yr

For the velocity file used, I also provide files with the horizontal and vertical velocities in the format expected by the GMT software psvelo (units cm/yr).

Alaska-seasonal-NOAM-vert.gmtvec
Alaska-seasonal-NOAM.gmtvec

Code and data files needed for computing forward model (requires MATLAB)

See Julie Elliott's copy of the report.